Available online at www.sciencedirect.com

jmr&t Journal of Materials Research and Technology

journal homepage: www.elsevier.com/locate/jmrt

Short Communication

Formation of nano-sized compounds during friction stir welding of Cu–Zn alloys: effect of tool composition

Akbar Heidarzadeh [a,*], *Amin Radi* [b], *Guney Guven Yapici* [b]

[a] *Department of Materials Engineering, Azarbaijan Shahid Madani University, Tabriz, 53714-161, Iran*
[b] *Mechanical Engineering Department, Ozyegin University, 34794, Istanbul, Turkey*

ARTICLE INFO

Article history:
Received 1 July 2020
Accepted 19 November 2020
Available online 27 November 2020

Keywords:
Friction stir welding
Cu–Zn alloys
Electron backscattered diffraction (EBSD)
Transmission electron microscopy (TEM)

ABSTRACT

For the first time, the origin of tool composition effect on microstructure and mechanical properties of the friction stir welded joints has been disclosed. For this aim, nano-indentation, orientation image microscopy, and transmission electron microscopy were employed to analyze the microstructure and mechanical properties in the case of copper-zinc alloy joints welded by different tool compositions. The results showed that the nano-sized intermetallic compounds were formed in the stir zone when using a hot-work steel tool, which increased the strength of the joint. The outcomes of this work can be used to modify the friction stir welded joints of various metals and alloys.

1. Introduction

Friction stir welding (FSW) of different metals and alloys has become a hot topic in recent years. To date, many researchers have investigated different aspects of FSW, in which the common goal is the structure-properties modification [1,2]. The FSW literature reveals that one of the most important parameters influencing the final microstructure and mechanical properties of friction stir welded (FSWed) materials is tool design [3]. In this regard, most of the researchers have focused on tool pin and shoulder profile design. However, the effect of tool composition on the microstructure and mechanical properties has been neglected. Therefore, a relevant question is whether the tool composition affects the microstructure and mechanical properties of the FSWed metals and alloys or not? To answer this question, two different tool compositions were used for FSW/P of a single phase Cu–Zn alloy and the FSWed materials were characterized using transmission electron microscopy (TEM) and nano indentation test.

2. Materials and methods

The base metal (BM) was a single phase brass plate with 30 wt.% Zn and dimensions of 150 × 100 × 2 mm provided form Farda-Negar Co. Two different tools were made of WC-

* *Corresponding author.*
E-mail addresses: ac.heydarzadeh@azaruniv.ac.ir, ak.hz62@gmail.com (A. Heidarzadeh).
https://doi.org/10.1016/j.jmrt.2020.11.058

Co and H13 hot work tool steel provided form Farda-Negar Co. The tools had same profiles, which were both composed of a cylindrical shoulder with a diameter of 12 mm and a simple cylindrical pin with a diameter of 3 mm and a length of 1.7 mm. The brass plates were FSWed under the equal process parameters using different tools of WC-Co and H13 tools. The rotational speed, traverse speed, and plunge depth was set constant at 450 rpm, 150 mm/min, and 0.2 mm, respectively. For the sake of briefness, the FSWed samples by WC-Co and H13 tools are coded as WC and H13 samples, respectively. It is notable that H13 tool was thermal treated to increase its hardness to 52 HRC.

For investigating the mechanical properties, nano-indentation tests were performed a MTS XP Nano-indenter (Oak Ridge, Tennessee, USA) equipped with a Berkovich diamond indenter. The reverse algorithm was used to extract the local mechanical properties (yielding strength σ_y and strain hardening exponent n) [4]. The microstructure of the joints was first examined by optical microscopy (OM-Tokyo, Japan), and orientation image microscopy (OIM). The OIM specimens were cross sectioned from the joints perpendicular to the FSW direction. The specimens for OIM were finalized after mechanical polishing by electropolishing for 30 s in a solution containing 250 mL H_3PO_4, 250 mL ethanol, 50 mL propanol, 500 mL distilled water, and 3 g urea at 10 V and 25 °C. A Philips XL30 E-SEM (USA) field emission gun scanning electron microscope equipped with an electron backscattered diffraction (EBSD) system was employed for OIM. The average grain size of the samples was calculated by OIM software according to ASTM standard. Transmission electron microscopy (TEM, JEOL JEM 2010-Tokyo, Japan) was used for more clarification of the microstructural details. For TEM sample preparation, the electrojet thinning was used with a solution of 30% H_3PO_4 and 70% distilled water at the applied potential of 80 V.

3. Results and discussion

The nano-indentation results showed that the yield strength (σ_y) and strain-hardening coefficient (n) were equal to 172 MPa/0.28, and 191 MPa/0.26, respectively for WC and H13 joints. In fact, the change of tool composition from WC to H13 has caused an increase of 11% in σ_y, and a decrease of 7.1% in n of the FSWed material. The macrographs of the joints are illustrated in Fig. 1, which show that both the joints were composed of distinct microstructural zones of base material (BM), thermomechanically affected zone (TMAZ), and stir zone (SZ). These macrographs show that both tools had similar effect on deformation and heat generation during FSW due to their equal geometries and dimensions [5,6].

The inverse pole figure (IPF) map, grain average misorientation (GAM) map, and (111) pole figures for the joints are illustrated in Fig. 2. From Fig. 2a, and d, the average grain sizes were 3.18 and 1.46 μm, respectively, for the WC and H13 samples. The GAM maps (Fig. 2b, and e) can be used for estimation of dislocation densities, qualitatively [7], in which the higher GAM values refer to higher internal energies. As seen, there was not a considerable difference between the GAM maps of WC and H13 samples, which indicated similar dislocation densities. In addition, the pole figures (Fig. 2c, and f) disclosed a shear texture type formed in the samples. The texture strength were also approximately equal in both samples. Thus, the only difference between the microstructures of the WC and H13 samples is their average grain sizes, in a way that H13 has caused finer grains.

It is well documented that the grain structure formation during FSW of brass alloys is governed by competition of two types of dynamic recrystallization (DRX) known as continuous and discontinuous dynamic recrystallization (CDRX and DDRX) [8,9]. Therefore, the fine grained structures of WC and H13 joints (Fig. 2) are due to occurrence of both the CDRX and DDRX during FSW. The grain size after DRX is a function of the "Zener-Holloman" parameter (Z), which is dependent on process parameters such as temperature and strain rate [10]. In addition, the chemical composition and physical properties such stacking fault energy (SFE) of metals and alloys can change the DRX grain sizes [10,11]. In this study, all the process parameters, chemical composition, and physical properties of the BMs were constant during FSW. The only parameter being altered was the tool composition.

In order to identify the effect of tool composition on the substructure of the samples, TEM analysis was used. The TEM images of the samples revealed considerably differences between the substructures (Fig. 3 and 4).

From Fig. 3, the substructure of WC joint contained grains with a high density of dislocations, which had tangled structures. This type of substructure in WC joint is frequently mentioned in literature [12]. However, in the case of H13 joint, in conjunction with a high density of tangled dislocations, some newly formed compounds with spherical morphology were observed as shown in Fig. 4a, and b. The EDS analysis

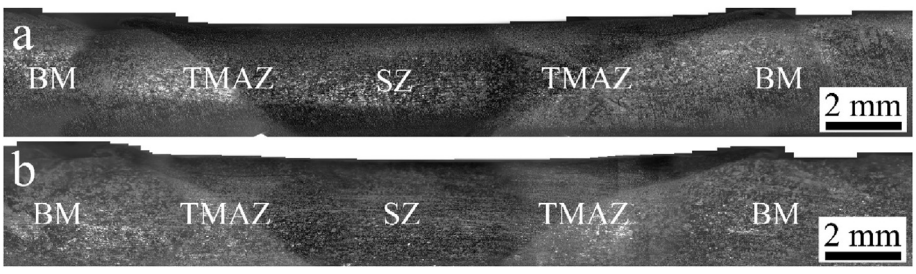

Fig. 1 – Macrographs of the joints welded using: (a) H13 tool, and (b) WC tool. The macrographs were produced by combining several OM images.

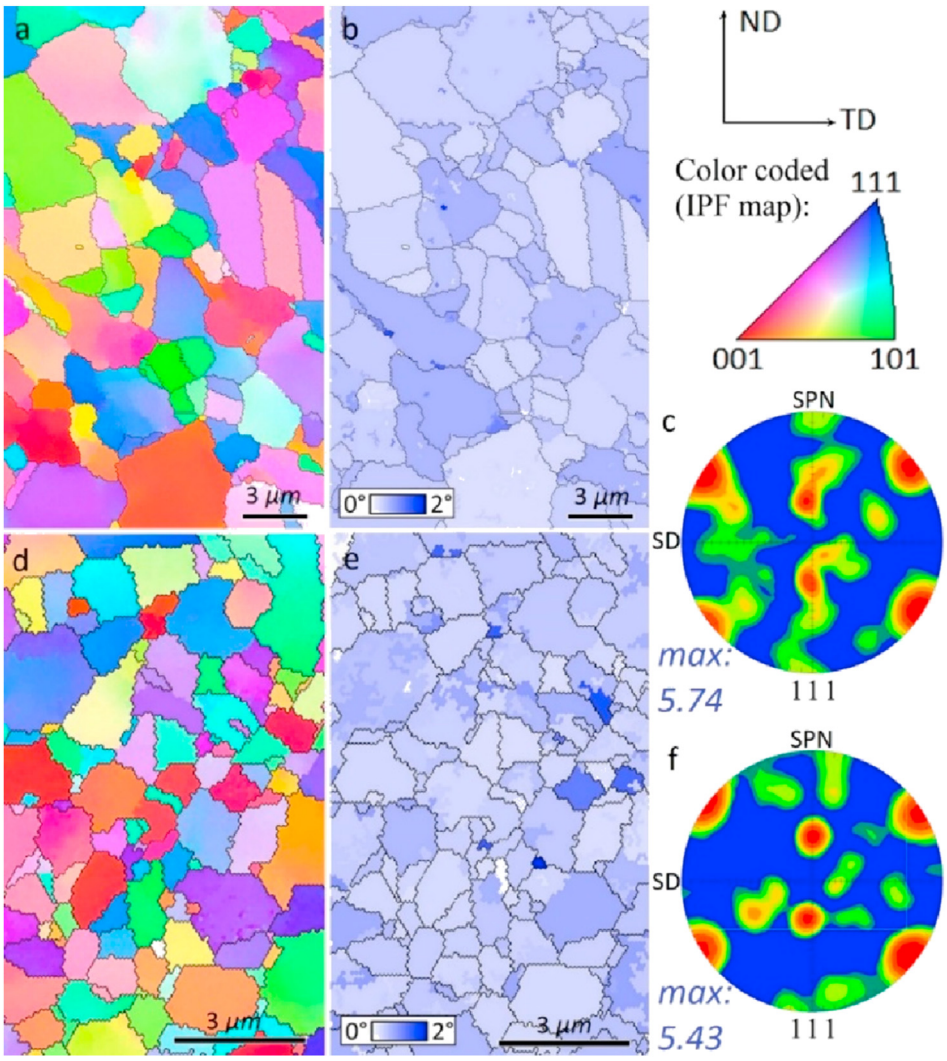

Fig. 2 – IPF map, GAM map, and (111) pole figures, respectively for (a–c) WC joint, and (d–f) H13 joint.

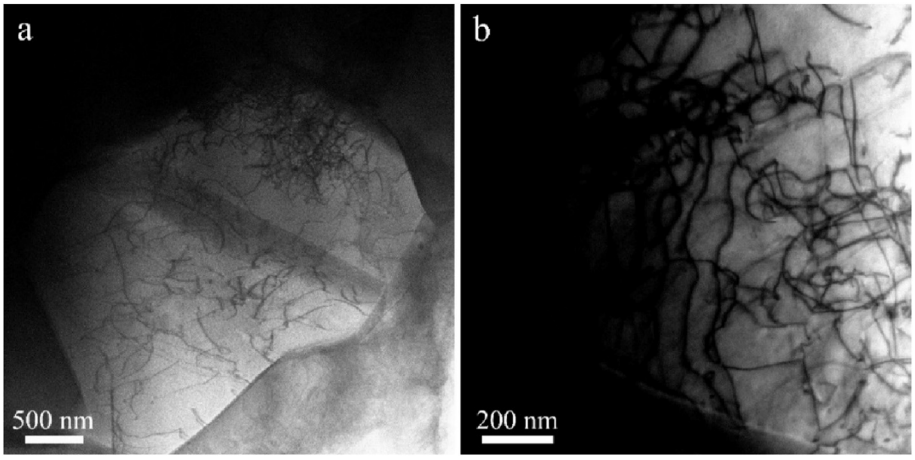

Fig. 3 – STEM images of the WC joint. (a) Formation of high density of dislocations with tangled structures inside the DRX grains. (b) High magnified image of dislocations.

(Fig. 4c) disclosed that the matrix contained only Cu and Zn, where the nano-sized compounds contained Cu, Zn, Fe, and Cr. It is notable that the amount of Cr was quite low in these compounds compared to other elements.

The formation of these compounds can be explained by a diffusion controlled mechanism due to two reasons. First, these compounds have a spherical morphology, and they can be formed from the debris of the tool. It is well documented

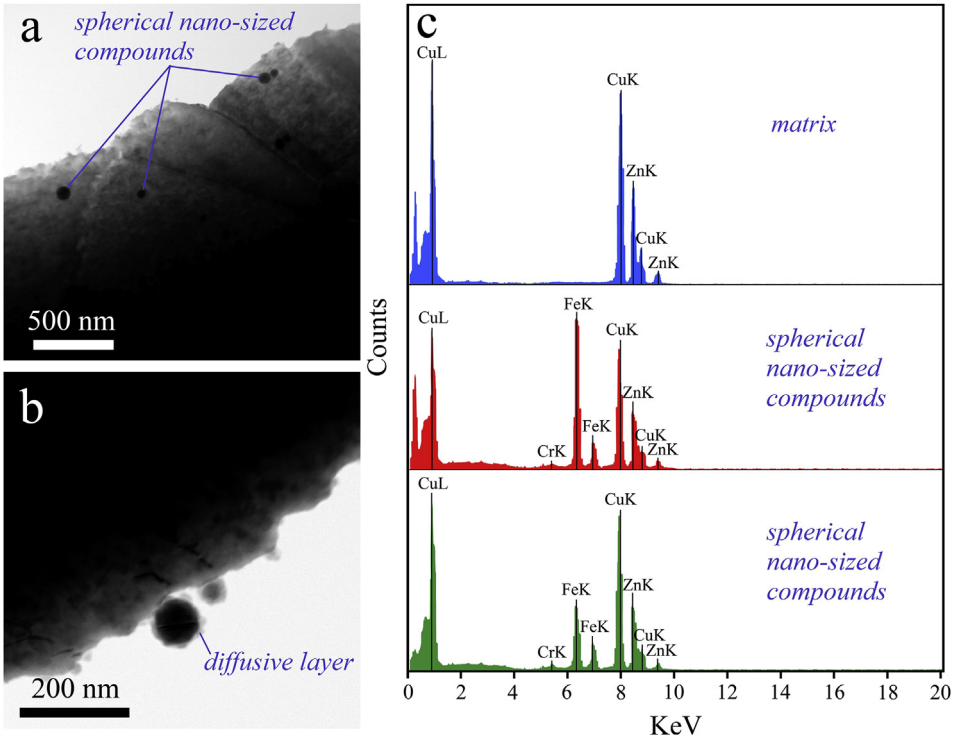

Fig. 4 – (a) Substructures of the H13 joint showing: (a) formation of spherical nano-sized compounds (see also Fig. 4b), (b) existence of a dissuasive layer around the nano-sized compounds, (c) EDS results for the matrix and nano-sized compounds indicated in (a) and (b).

that during FSW of hard materials, tools are damaged due to severe plastic deformation, and the tool wear causes the travelling of tool debris into the joints [13]. These debris have irregular shapes and are not to be the source of detected CuZnFeCr compounds. Secondly, there are diffusive interlayers which are formed between the matrix and the spherical compounds as marked in Fig. 4b. Therefore, it can be concluded that Fe and Cr have dispatched from the tool during FSW, and then they have traveled inside the joint to combine with Cu and Zn. The spherical morphology of the formed compounds is due to their low surface energy, which makes them stable from the thermomechanical view point.

The TEM images had also shown the origin of finer grain sizes of H13 joint compared to WC joint. The spherical nano-sized compounds were detected on the grain boundaries, as shown in Fig. 5a. After grain structure formation during FSW by CDRX and DDRX mechanism, the DRX grains experience a growth step [11]. The nano-sized compounds pin the grain boundaries during growth step as shown in Fig. 4a, and leads to a reduction in their mobility. Thus, nano-sized compounds inhibit the growth of DRX, and hence the finer grain sizes are formed in the H13 joint. Similar mechanisms have been reported in the case of two phase alloys such as duplex brass alloys [12].

From the viewpoint of strengthening mechanisms, nano-sized compounds had increased the strength of H13 joint due to the following mechanisms, which confirm the nano-indentation results. Firstly, nano-sized compounds caused finer grain sizes, and hence larger area of grain boundaries. Grain boundaries act as obstacles to dislocation movement during deformation, and thus the strength of metals and alloys increase by a reduction in their grain sizes according to $\sigma_y = \sigma_0 + k_y d^{-1/2}$ (Hall–Petch equation). In Hall–Petch equation, σ_y is yield strength, σ_0 refers to the single crystal strength, k_y is constant, and d stands for grain size. Secondly, nano-sized compounds pin the dislocations as shown in Fig. 5b. It is well established that the pinning of dislocations by secondary phases leads to a reduction in their mobility, and hence the strength increases, which is known as load bearing effect ($\Delta\sigma_{LB}$). In the load bearing effect ($\Delta\sigma_{LB}$), high density of dislocations around the reinforcements results in large plastic strain fields, and hence large amount of applied stress is needed to continue the deformation. $\Delta\sigma_{LB}$ can be formulated as follows [14]:

$$\Delta\sigma_{LB} = VF_{RE}\left(S/A\right)\left(\tau_a/2\right) + \sigma_a VF_a \quad (1)$$

The diffusive layer around the nano-sized compound is obvious, which confirm the previous explanations. Thirdly, stacking faults (SFs) were detected inside the larger nano-sized compounds as shown in Fig. 5c. In Fig. 5d, the HRTEM image of nano-sized compounds is also shown. Therefore, the new compounds are deformed by the formation of SFs inside them, which cause strengthening of the matrix. In addition to the mentioned mechanisms, the other mechanisms are also probable mechanism according to the literature. In equation 2, VF_{RE} and VF_a are volume fraction of reinforcements and matrix, respectively. σ_a and τ_a are yield and shear strengths of matrix. S and A refer to the interfacial

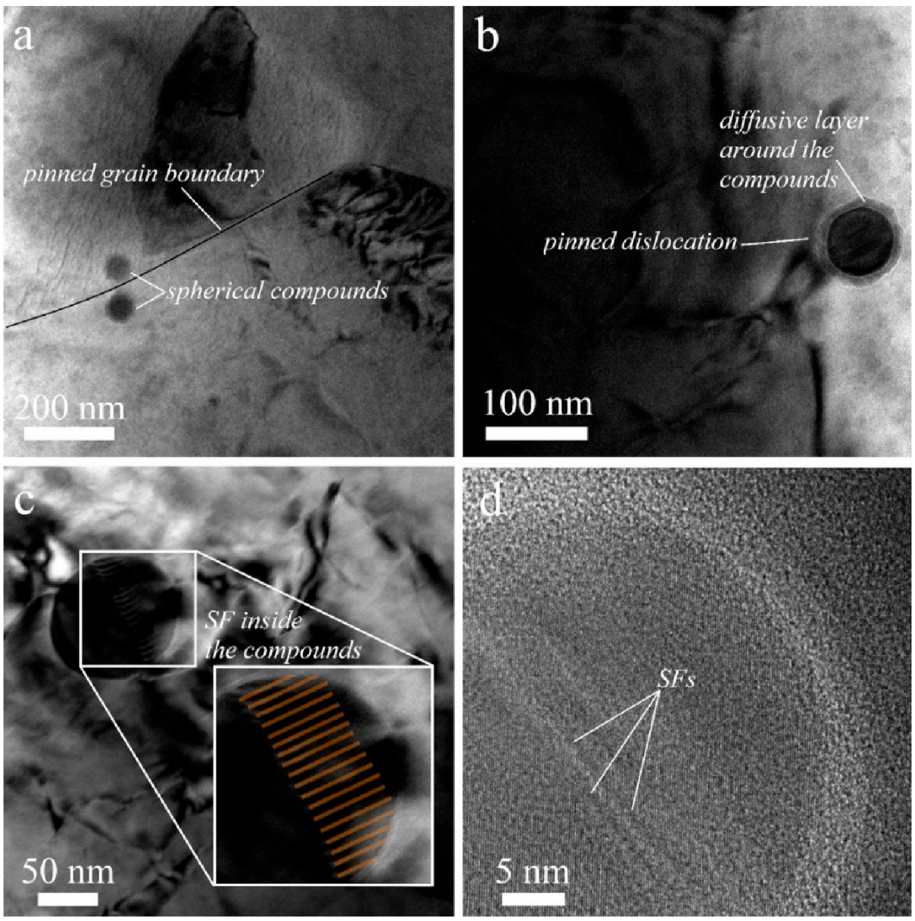

Fig. 5 – (a) STEM image showing grain boundary pinning by nano-sized compounds in H13 joint, (b) STEM image showing dislocation pinning, (c) STEM image and (d) HRTEM image showing formation of SFs inside the nano-sized compounds.

and cross sectional area of reinforcements. Furthermore, the difference between thermal coefficient of matrix and reinforcements cause to production of dislocations during cooling cycle of process, which is called usually thermal mismatch mechanism ($\Delta\sigma_{TM}$). Thermal mismatch mechanism is one of the main mechanisms leading to higher yield strength in composites in which the generated geometrically necessary dislocations results in work hardening [15]. Moreover, the Orowan mechanism ($\Delta\sigma_{OR}$) can also contribute in strengthening of composites. In this mechanism, interaction of moving dislocations with reinforcements causes bending of dislocations and produces back stresses, which hinders migration of dislocations [16]. In summary, H13 joint had higher strength than WC joint due to grain boundary, dislocation pinning, and SF strengthening mechanisms induced by nano-sized compounds.

4. Conclusion

Different WC-Co and H13 steel tools were used for FSW of Cu–30Zn plates, and the following conclusions can be summarized. Using H13 tool causes higher strength in the joint due to following mechanisms. During FSW, Fe and Cr travel from the tool surface into the CuZn matrix, and they form nano-sized intermetallic compounds. These compounds pin the DRX grain boundaries, and inhibit their mobility and grain growth leading to finer grain sizes. In addition, nano-sized intermetallics pin the dislocations, and reduce their mobility. Moreover, SFs are formed in the atomic structure of these compounds. In summary, tool composition has a considerable effect on the microstructure and mechanical properties of the joints. The outcome of this study can be utilized in designing FSW tools suitable for joining different metals and alloys.

Data availability

The raw/processed data required to reproduce these findings cannot be shared at this time due to legal or ethical reasons.

Declaration of Competing Interest

The authors declare that they have no known competing financial interests or personal relationships that could have appeared to influence the work reported in this paper.

Acknowledgments

Akbar Heidarzadeh would like to thank the Fardanegar Knowledge-based Company (FKC) for their technical support to conduct the experiments. In addition, partial support of Ozyegin University Research Fund is acknowledged.

REFERENCES

[1] Heidarzadeh A, Mironov S, Kaibyshev R, et al. Friction stir welding/processing of metals and alloys: a comprehensive review on microstructural evolution. Prog Mater Sci 2020:100752. 2020/10/08/.
[2] Nandan R, DebRoy T, Bhadeshia HKDH. Recent advances in friction-stir welding–process, weldment structure and properties. Prog Mater Sci 2008;53(6):980–1023.
[3] Mishra RS, Ma ZY. Friction stir welding and processing. Mater Sci Eng R Rep 2005;50(1–2):1–78.
[4] Dao M, Chollacoop N, Van Vliet KJ, et al. Computational modeling of the forward and reverse problems in instrumented sharp indentation. Acta Mater 2001;49(19):3899–918. 2001/11/14/.
[5] Meng X, Huang Y, Cao J, et al. Recent progress on control strategies for inherent issues in friction stir welding. Prog Mater Sci 2021;115:100706. 2021/01/01/.
[6] Ji SD, Wen Q, Li ZW. A novel friction stir diffusion bonding process using convex-vortex pin tools. J Mater Sci Technol 2020;48:23–30. 2020/07/01/.
[7] Tehrani-Moghadam HG, Jafarian HR, Heidarzadeh A, et al. Achieving extraordinary strength and ductility in TRIP steels through stabilization of austenite up to 99.8% by friction stir welding. Mater Sci Eng, A 2020;773:138876.
[8] Mironov S, Inagaki K, Sato YS, et al. Development of grain structure during friction-stir welding of Cu–30Zn brass. Phil Mag 2014;94(27):3137–48.
[9] Heidarzadeh A, Saeid T. A comparative study of microstructure and mechanical properties between friction stir welded single and double phase brass alloys. Mater Sci Eng, A 2016;649:349–58. 2016/01/01/.
[10] Sakai T, Belyakov A, Kaibyshev R, et al. Dynamic and post-dynamic recrystallization under hot, cold and severe plastic deformation conditions. Prog Mater Sci 2014;60:130–207.
[11] Humphreys FJ, Hatherly M. Recrystallization and related phenomena. Elsevier; 2004. Edition n, editor.
[12] Heidarzadeh A, Chabok A, Klemm V, et al. A novel approach to structure modification of brasses by combination of non-equilibrium heat treatment and friction stir processing. Metall Mater Trans 2019;50(5):2391–8.
[13] Torganchuk V, Vysotskiy I, Malopheyev S, et al. Microstructure evolution and strengthening mechanisms in friction-stir welded TWIP steel. Mater Sci Eng, A 2019;746:248–58.
[14] Rashad M, Pan F, Asif M, et al. Powder metallurgy of Mg–1% Al–1%Sn alloy reinforced with low content of graphene nanoplatelets (GNPs). J Ind Eng Chem 2014;20(6):4250–5. 2014/11/25/.
[15] Magnus C, Sharp J, Ma L, et al. Ramification of thermal expansion mismatch and phase transformation in TiC-particulate/SiC-matrix ceramic composite. Ceram Int 2020;46(12):20488–95. 2020/08/15/.
[16] Szajewski BA, Crone JC, Knap J. Analytic model for the Orowan dislocation-precipitate bypass mechanism. Materialia 2020;11:100671. 2020/06/01/.